MODELLING OF IMPACT ON SANDWICH STRUCTURE FOR FAST MAINTENANCE LOOPS

B. Castanié*, Y. Aminanda† and C. Schwob**
***Institut Clément Ader, Toulouse France, † IIUM Kuala-Lumpur, Malaysia**
**** EADS Innovation Works, Aerospace Malaysia Innovation Centre (AMIC) Kuala Lumpur, Malaysia**
bruno.castanie@insa-toulouse.fr yulfian@iium.edu.my cyrille.schwob@eads.net

Keywords: *composite, sandwich, impact,*

Abstract

In the aeronautical field, sandwich structures are widely used for secondary structures like flaps or landing gear doors. The modeling of low velocity/low energy impact, which can lead to a decrease of the structure strength by 50%, remains a designer's main problem. Since this type of impact has the same effect as quasi-static indentation, the study first focuses on the behavior of honeycomb cores under compression. A phenomenological analysis was conducted which highlights the postbuckling behavior of the honeycomb structure thus enabling a discrete modeling. This discrete approach accurately predicts the static indentation on honeycomb core alone, the indentation and the residual dent depth on sandwich structure with metal skins supported on rigid flat support. The domain of validity of this approach is investigated. In any case, the spring elements used to model the honeycomb cannot take into account the transverse shear that occurs in the core during the bending of a sandwich. To overcome this strong limitation, a multi-level approach is proposed. Thus, it is possible to predict the dynamic structural response in the case of low-velocity/low-energy impact on metal-skinned sandwich structure in bending. A good correlation with dynamic experimental tests is achieved. This model is then used to simulate the response of this indented structure subjected to lateral compressive loading (known as CAI/ Compression after impact). A good correlation with test results is obtained except for the very small residual print depth. To predict the residual strength of impacted sandwich, a core crush criterion is proposed and validated first with metallic skins and then with composite skins.

1 Introduction

Sandwich structures exhibit static properties such as high stiffness-to-weight ratio and high buckling loads which are of great importance in the aeronautics field. Nevertheless, the current applications on commercial airplanes remain mainly limited to secondary structures like control surface or floor panels. In the field of helicopters where stress levels are lower, full sandwich structures are already in flight. In fact, one of the main limitations is linked to a lack of knowledge on the effects induced by impact damages [1]. However, in service, such structures are exposed and are often impacted during taxiing or take-off. It can also be damaged by tool drops during maintenance operations. In such circumstances, the aircraft manufacturer has to inform the users very quickly of whether the impacted structure needs a repair or not. The study presented in this workshop is a step toward the final objective, which is to provide the aerospace industry with an inverse method. In this method, a 3D picture of the damage is first made by the airline company. Then, based on the shape of the impact, the impactor's shape is found and both the impact damage and the residual strength would be computed as quickly as possible.

The different steps of the analysis presented hereafter are:

- A phenomenological study of the honeycomb core crushing which lead to an original modeling approach.
- The analysis of the impact on sandwich plate with metallic skins fully supported and the enhancement of the model to take into account the interaction between the skin and the core.
- To overcome the limitation of the original finite element model developed, a multi-level approach is proposed.
- The compression is then studied and an original core crush criterion is identified with metallic skins and then validated with composite skins.

2 Phenomenologigal analysis of core crushing and discrete modelling

The mechanism of crushing was first observed by a camera on a honeycomb made of paper with large cell size [2] glued to one or two Plexiglas skins. Then, the crushing of Nomex and aluminum honeycomb was analyzed. It was shown that the boundary conditions play an important role. This experimental study highlights the importance of the vertical edge behavior which controls the crushing laws after the local buckling of the cell wall. Also, this buckling force corresponding to this mode is about 20 to 50% of critical force observed on testing. The numerical analyses seem to confirm the interpretation of the test results. Since local buckling occurs early (only for soft cores, not for aluminium core), the honeycomb structure works in a postbuckling mode and an analogy can be made with stiffened structures under compression in aircraft (Fig. 1).

The stiffener in honeycomb is the vertical edge that is formed by the intersection of three cell walls. When the skin buckles, the compressive stress in the skin cannot be more than the buckling stress and the compression excess is therefore taken up by the stiffener and the nearby skin, with an equivalent half-width equal to 15 times the skin thickness. By analogy, for the honeycomb cell, the compression is mainly taken by the vertical edges since the buckling of the walls occurs earlier. Then the collapse of the stiffened structure corresponds to the buckling of the stiffeners. In the case of honeycomb there is no collapse, but rather folding. The previous analysis shows that only the cell edge plays an important role from a structural point of view. This reasoning leads to the hypothesis that Nomex^{TM} honeycombs under a crushing force behave like a juxtaposition of vertical cell edges and it is possible to model them by a grid of vertical nonlinear springs located at the angles of the hexagons. This hypothesis was validated by comparison with several indentation tests on Nomex^{TM} honeycombs with spherical indenters with different radii

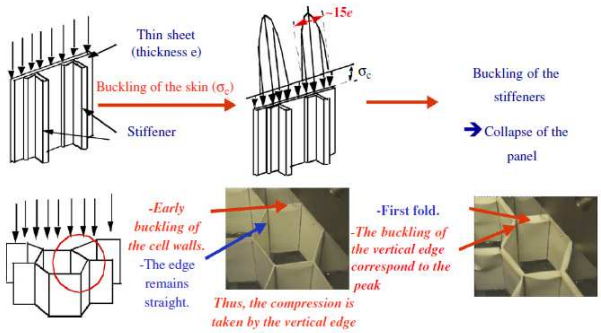

Fig. 1. Analogy with the buckling of stiffened panels.

3 Analysis of impact on metal-skinned plates.

Experiments and numerical studies were carried out on sandwich structures with metal skin and Nomex^{TM} honeycomb. Metal skins were used in order to avoid the complex failure damage mode of composite laminated skin. Quasi-static indentation test were carried out on 100x100mm^2 sandwich structures. Brass skins of 0.1 and 1mm thickness were bonded to the honeycomb. Indentation of all specimens was done using the same INSTRON^{TM} machine and the same spherical indenters having different radii (57.25, 30.125 and 21.75 mm). The specimens were fully supported on a rigid metallic part (Fig. 2). An implicit nonlinear finite element model was made (see Fig. 3). Nonlinear springs were placed at the same location as the honeycomb cell angles. A generalized law was implemented which takes into account the skin/honeycomb interaction [3].

Fig. 2. Description of the indentation tests on sandwich specimens.

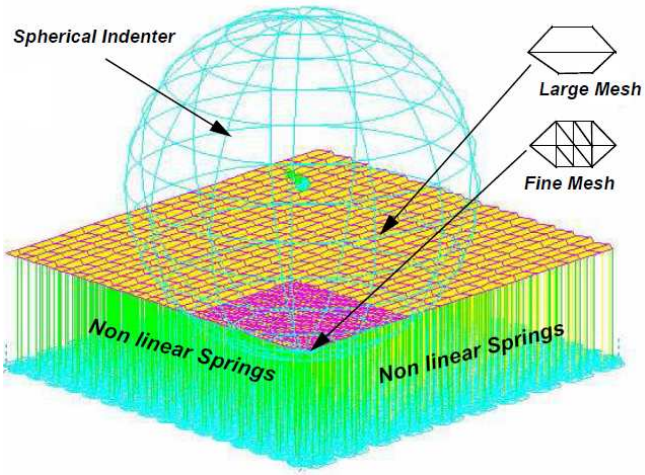

Fig. 3. Finite element modeling of the indentation problem on sandwich with thin metal skins.

The results of computation were compared to the tests on sandwiches with thin skins and a good test/computation comparison was obtained for all three indenter radii. Globally, the undulations observed during the tests were also found numerically and corresponded to the drop in the load after the peak load of each vertical edges located at the circumference of the indented area. When a honeycomb sandwich structure undergoes bending, the transverse shear of the core plays an important part in the deflection and has to be taken into consideration. It is obvious that the proposed modeling of the core by a series of nonlinear vertical springs cannot take this transverse shear stress into account. However, it was demonstrated in [3] that the bending and indentation effects are uncoupled. Physically, this uncoupling can be attributed to the existence of a plasticized area at a very early stage, under the indenter area. This area becomes saturated in stress and insensitive to the loading increments on the sandwich skin. The only possible coupling must appear at the initiation of the indentation area, which must logically be earlier when the skin is loaded under lateral compression. However, this phenomenon was not observable for the configuration tested. Thus, it is possible to propose a multi-level approach (see Fig 4) to compute the response of a sandwich structure subjected to dynamic impacts.

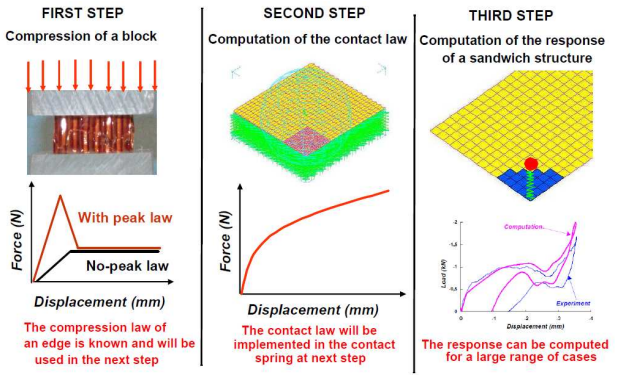

Fig. 4. Multi-Level Approach for the Modeling of Impact on Sandwich Structures.

This approach was validated by dynamic tests on simply-supported sandwich plates [3].

4 Residual dent and post-impact behavior.

In this section, the discrete approach proposed in the previous section will be used to make a complete computation loop including indentation, computation of the residual print geometry and computation of the compression after indentation (CAI) strength. In this part, the approach is limited to a sandwich with metallic skins. Nevertheless, the discrete approach allows identifying the failure mechanisms during CAI and the role of core crushing before the collapse of the sandwich panel. Thus, a core crush criterion can be identified [5].

Specimens (Fig. 5) were prepared by taking care to obtain high surface smoothness and high dimensional precision which are the necessary conditions to obtain a correct uniform compressive test. The standard dimension of the specimen was 150x100 mm^2. Two brass skins (thickness 0.5 mm) were bonded to Nomex honeycomb core HRH 78,1/4,3 (thickness 15 mm). Resins were molded into both extremities of each specimen. To transfer the compressive load properly, two plates were added as reinforcement in the resin–Nomex junction area.

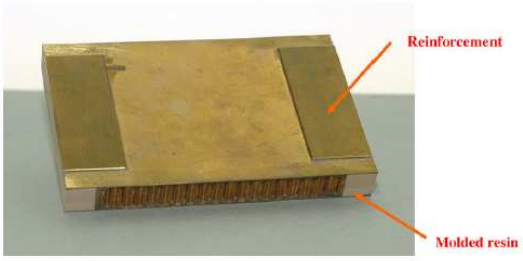

Fig. 5.Specimen for CAI test

These specimens were previously indented on a flat support and the indentation was carried out by imposing a displacement with a constant speed of 0.5 mm/mn. A spherical indenter made of steel with radius of 57.25 mm was used and several depths of maximum indentation d = 0, 0.5, 1, 1.5 and 2 mm were used to obtain different damage areas. For compression (CAI) tests after indentation, test supports and specimens corresponded to the AIRBUS standards so that we could compare the test results with industrial ones. To observe the evolution of damage geometry in terms of its depth and its form during compressive loading, a method of 3D Image correlation using two cameras was employed (Fig. 6). Strain gauges were also used to observe the distribution of compression flux on the two skins. The compressive load acting on the specimens was measured directly from the INSTRON machine and the displacement of the compression surface was measured using LVDT displacement measurement.

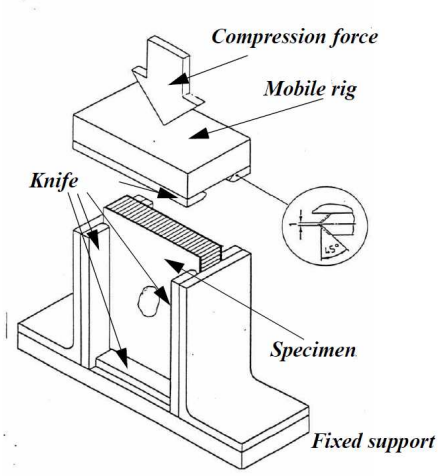

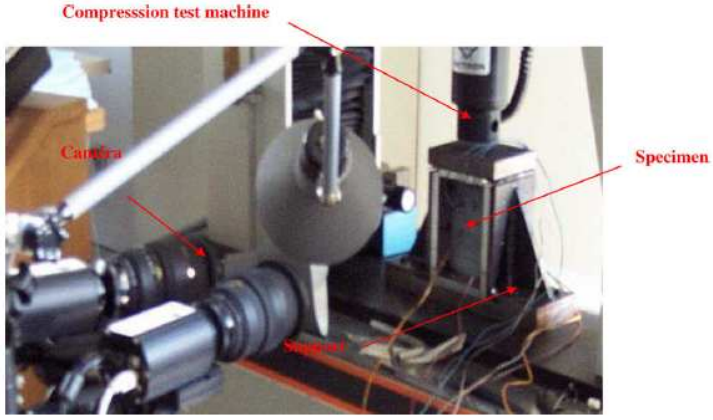

Fig. 6. CAI test device.

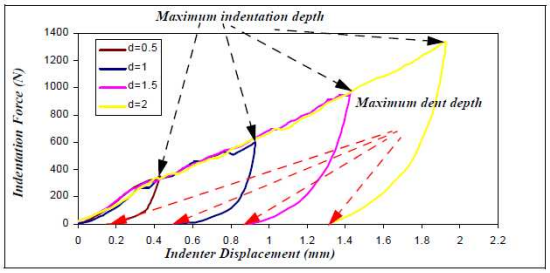

Fig. 7. Force / displacement curves using an indenter of radius R = 57.25 mm.

The experimental contact laws are plotted in Fig. 7. We note that the relaxation phenomenon is highly nonlinear and that the difference between the depth of the residual dent and the maximum depth of the indentation is significant. Qualitatively, although the depth of the residual print is very small, it can come from a significant indentation that has generated significant honeycomb crush. Furthermore, we observe that the relative difference is not constant and decreases as the depth of the indentation increases

By observation using Digital Image Correlation (DIC), Fig. 8, the evolution of the damage area can be described as follows:

- In the region of elastic behavior of the skins, the shape of the residual print geometry after indentation remains circular and its depth hardly varies.
- At the beginning of plastic behavior of the skins, the form of the print begins to become elliptical, progressively, in the direction of lateral axis a. At the same time, in the direction of longitudinal axis, b, no evolution is observed. The print depth is also observed to increase progressively.

• Approaching maximum compressive load (residual strength of the structure), the print depth increases abruptly. The same observation is also obtained for the evolution of radii about the lateral axis, a, which finally reach the edges of specimen. It is also interesting to note that the deflection of non-indented skin below the indented area also increases rather quickly.

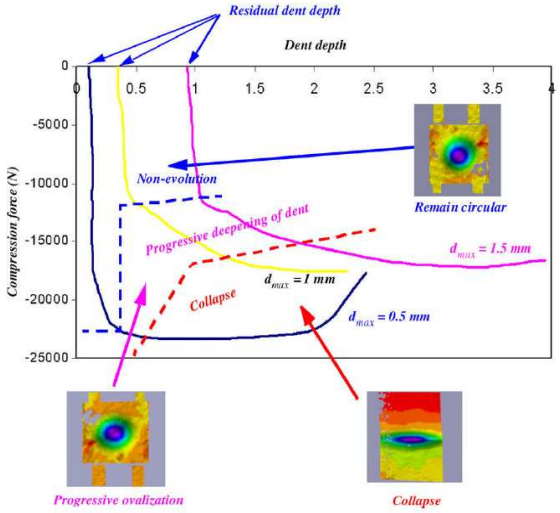

Fig. 8. Evolution of the dent under compression after impact loading for maximum dents dmax of 0.5, 1 and 1.5 mm and identification of different behaviors with the help of DIC.

For the specimen that was indented only with maximum indentation depth d = 0.5 mm and which had a corresponding residual print depth of 0.1 mm, the evolution of the damage geometry was quite different. This specimen, with only 2% of decrease in terms of residual strength, behaved almost as a non-indented specimen. However, the elliptical evolution of the damage geometry was also observed with an abrupt progression when approaching the maximum compressive loading. This behavior was similar from all qualitative points of view to that observed for a thin composite skin.

Globally, the same finite element model using implicit SAMCEF software that was used for the study of indentation was employed here (see Fig. 9).

The principles of the model are as follows:

Indented skin is modeled by Mindlin-type elements. This skin has free boundary conditions except at the position of the CAI test supports (z-axis degree of freedom (d.o.f.) locked). These boundary conditions did not exist during indentation. However, the literature shows that indentation causes a local damage area and, for the size of specimen used in this study, the boundary conditions are not sensitive. This insensitivity was confirmed by a posteriori numerical computation. The compression law for the brass skin was obtained from tests on a virgin (non indented) sandwich specimen and it appeared that the yield stress in compression was 110 MPa instead of the 100 MPa obtained for traction. Also, the hardening law was slightly different

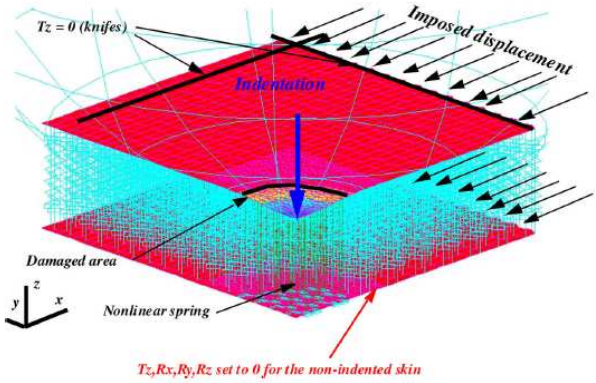

Fig. 9. Finite element model for compression after impact.

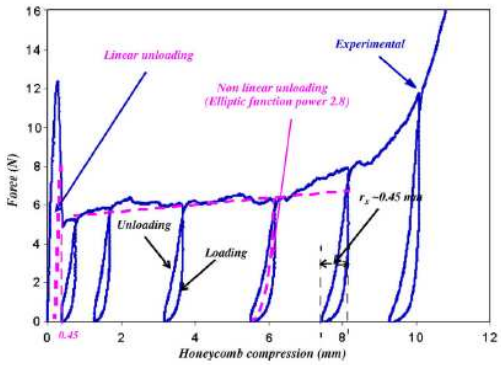

Fig. 10. Compression behavior of Nomex honeycomb with cycling.

• Hexagonal Nomex honeycomb was modeled by a grid of non-linear vertical springs placed geometrically at the same positions as the honeycomb vertical edges. Its behavior law was obtained experimentally from a cycled compression uniform loading test on a small block of Nomex honeycomb (Fig. 10). Until 0.4 mm of displacement of the uniform compression surface, compression unloading gave a linear return of displacement with the same slope as the compression one. Beyond that displacement, the return was no longer

linear (ellipse with a power of 2.8). The hysteresis behavior found from the test was assumed negligible and was not taken into account in the FEM computation.

- Non-indented skin had to be modeled with the same model as indented skin but almost all the degrees of freedom were blocked, except for its in-plane displacement (in this case translation in x and y) to allow non-indented skin to deform like a membrane during compression.

The lower skin was added because the distribution of the forces between the two skins varied as the defect progressed. It is obvious that the discrete model used before cannot directly represent the bending of the sandwich and, hence, the out-of-plane displacement of the non-indented skin. In fact, all the degrees of freedom of this skin were locked except for the displacements in the plane of the sandwich (x and y axis) so that the skin could deform during the compression. However, this assumption was justified because the deflection of non-indented skin below the indented area measured during tests was very small and became significant only when the compressive load approached the maximum one. Also, globally, the deflection of non-indented skin still remained negligible compared to the depth of the indented area. Moreover, the computation was more robust numerically when the boundary conditions were conserved for complete computation involving different phases. The load acting on a structure was simulated by imposing first a vertical displacement of the indenter towards negative Z (compression loading) and positive Z (compression unloading), then followed by imposing the displacement on the edges of the structure to simulate the lateral compression load (CAI) on the indented structure.

The comparison between test and computation during the indentation phase is described in Fig. 11 for the case of maximum indentation d = 2 mm. The curve of indentation force as a function of indenter displacement is plotted in Fig. 11a and the profile of the residual print about the longitudinal axis b is plotted in Fig. 11b. The depth of the residual print obtained from the computation is 1.42 mm whereas 1.32 mm is obtained from the test measurement, which gives the difference of 7%. For all specimens, the difference of residual print between computation and test varies from 25% for the smallest indentation depth (d = 0.5 mm) to 7% for the deepest one (d = 2 mm). The curves obtained from the indentation test are correctly simulated by computation and also globally for the geometry of the residual print after indentation.

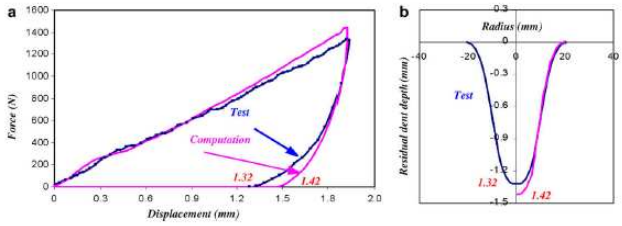

Fig. 11. Contact law and residual dent test compared with computation for a maximum indentation of 2 mm.

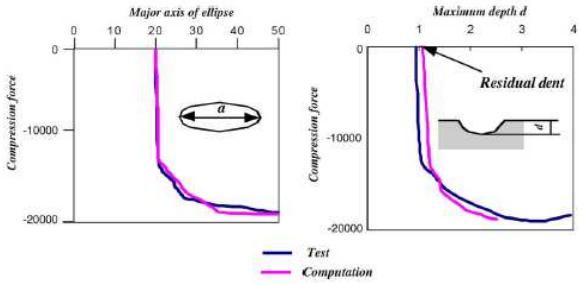

Fig. 12. Correlation of the maximum depth and the major axis of the ellipse of the dent during compression for the maximum indentation depth of 1.5 mm.

In the compressive loading after indentation phase, the evolution of the residual print was studied by analyzing two parameters: depth of residual print and profile about the major axis, a. The minor axis did not vary significantly. Test/computation comparisons for these two parameters are represented in Fig. 11 for the specimen indented with maximum indentation d = 1.5 mm. Globally, numerical computations give the same evolution as test results. The small difference at the beginning of the compression is due to the difference of residual print depth between computation and test from the previous phase. A good correlation between test results and computations in terms of print geometry evolution and maximum compressive load was obtained for almost all indented specimens except in the case of small indentation d = 0.5 mm [7].

5 Failure Mechanisms and core crush criterion.

In this part, the reaction of the first uncrushed springs placed in the dent evolution direction about the major axis of the ellipse and in the circumference of the residual print (see Fig. 13) is analyzed. The force in these springs (1–3) is initially low and does not increase during the appearance and progressive extension of the ellipse. After a drop in the spring force, which is due to the appearance of a bump at the periphery of the ellipse that stretches the springs, a sudden increase in the compression force is observed until it reaches the critical force (the peak) for the first spring at the periphery (no. 1). The collapse of this first edge occurs only shortly before the abrupt progression of the ellipse, which takes place when the second edge (spring no. 2), situated on the major axis of the ellipse, collapses in turn. Numerically, it is shown here that the advance of the defect coincides with the physical phenomenon of local core crush.

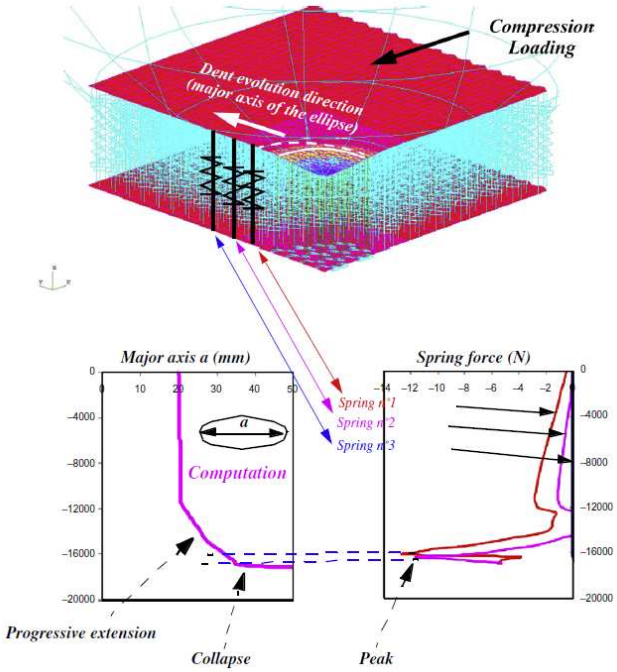

Fig. 13. Analysis of the collapse of pristine core after impact.

Therefore, ***the collapse of the first edge located on the major axis of the ellipse modeled by its spring can be proposed as the criterion for determining the computed residual strength***. Logically, this criterion should always underestimate the experimental residual strength, but not too much, since the ellipse generally appears just before the catastrophic failure of the specimens [6-7].

Thus, the analysis of the tests combined with the discrete modeling of the core shows that the phenomenon occurring during CAI is due to interaction between three mechanical behaviors:

- A geometrical nonlinearity due to the skin's neutral axis offset in the dent area.
- A nonlinear response of the core due to the crushed state and the classic ''with peak" response of the undamaged area.
- The response of the skin due to its type of damage after impact: plasticity for metallic skins and delamination or crack growth for laminated skins.

6 Application to sandwich structures with composite skins.

In this section, the discrete model is applied to the case of compression after impact on sandwich structures with composite laminate skin. The core crush criterion presented in the previous subsection will be used to evaluate the CAI strength. The difficulty in modeling the phenomena lies in the determination, a priori, of the damage area of the core and the skin according to the delamination area and geometry of impact. In practice, these data could be the input recorded during S.H.M of the structure. The model developed here is inspired by the works of Lacy and Hwang [8, 9] which demonstrate the ability to model the behavior of laminate sandwich structures after impact globally. In this study, the initial damage geometry after impact was measured directly from the specimen using destructive and non-destructive inspection. A fixed behavior law for composite skins was also used on the impacted area (50% of module degradation). In the following subsections, the model used in this study will first be described and then a comparison will be made with the tests results provided by the same authors [7-9].

Only a quarter of the plate was modeled due to symmetries and the overall shape as shown in Fig. 13. Thus the model size area was 101.6 x

127 mm^2. The geometry parameters of the impact-damaged area are described in Fig. 14 using the same notations as in [8, 9]. For all specimens reported here, the thickness of the core t_c was 19.1 mm. The facesheet indentation depth, d_I, and radius, R_I, could be measured directly on specimens or on a real structure. In the new finite element model, the geometry of the dent is represented by Coons surfaces. The crushed core radius should be found by NDI techniques. It seems to be more difficult, in the case of sandwich structures, to determine the delaminated area precisely. Thus, the degraded facesheet radius R_F will be taken to be equal to:

$$R_F = \frac{R_I + R_C}{2} \qquad (10)$$

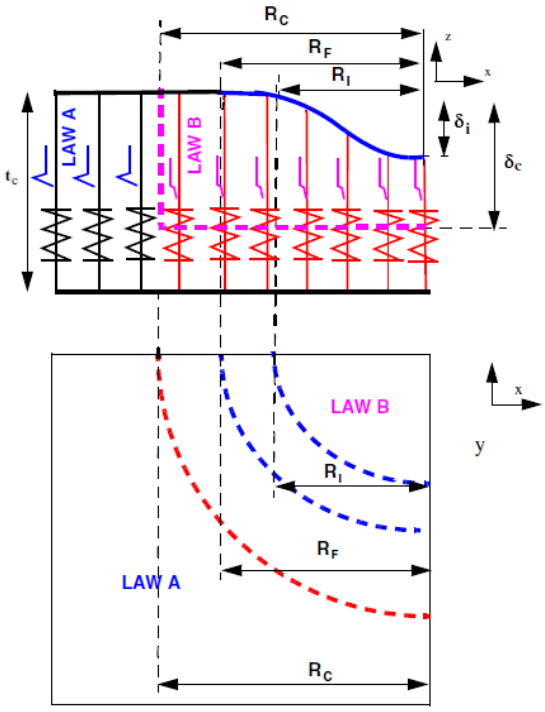

R_I : facesheet indentation radious
R_f : dagraded facesheet radious
R_C : crushed core radious
δ_I : facesheet indentation depth
δ_C : crushed core depth
t_C core thickness

Fig. 14. Geometry of the impact-damaged region.

The core used was made of Nomex honeycomb, 48 kg/m3 and had a cell size of 4.76 mm and a transverse modulus E equal to 137.9 MPa. Its maximum compressive strength was 2.41 MPa and the plateau stress was 1.03 MPa. Knowing all these values, for a given surface, it was easy to transform the continuum values into discrete ones for the springs located at the corners of the cells. Law ‘‘A” for an intact honeycomb under compression is given in Fig. 15.

The peak force was found to be 23 N and the crush force was 9.86 N. The compression displacements were calculated directly from the strains given in [8]. This law was applied to the springs representing the pristine core, i.e. located at a radius $R > R_C$.

.

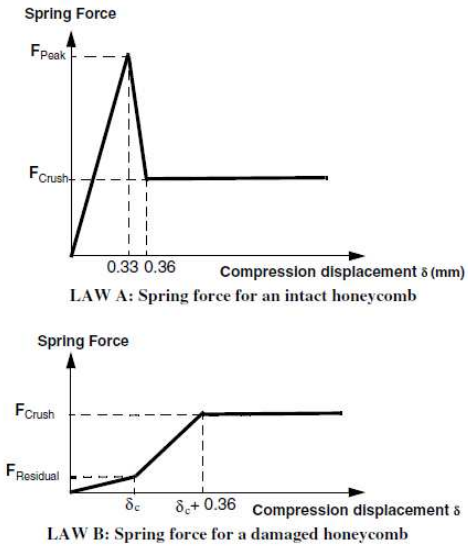

Fig. 15 . Spring forces.

For the springs representing the crushed core, law ‘‘B” was applied. These laws are of same type as in [8] and are in accordance with a previous cycling test performed by the authors on Nomex honeycomb (see Fig. 10). The true value of the crushed core depth δ_C was, until now, obtained by destructive sectioning. In an initial approach, the values given in [8] will be taken and applied to all springs located in the crushed area (see Fig. 14). When this is done, the evolution of the crushed depth is not represented but an a posteriori sensitivity analysis will demonstrate that the influence of this parameter is weak. The residual force $F_{Residual}$ is also a weak parameter and was set to 1 N, mainly for numerical stability reasons.

The skin was modeled by orthotropic Mindlin elements (see Fig. 13). The stacking sequence was [90/45]n with n = 1,2,3. Thus the skin thickness was equal to 0.4, 0.8 or 1.2 mm. According to the material characteristics of the ply given in [8], the orthotropic equivalent moduli were calculated and implemented in the

finite element model for the element located at a radius $R > R_F$: $E_1 = E_2 = 47{,}200$ MPa, $E_{12} = 17{,}800$ MPa, $G_{12} = 17{,}800$ MPa, $\nu_{12} = 0.328$. The same transverse characteristics as in [8] were implemented. For the damaged area, specific hypotheses were assumed concerning the stiffness matrix terms. For a given stacking sequence and for Mindlin's theory, this matrix can be written as:

$$\begin{bmatrix} A & B & 0 \\ B & D & 0 \\ 0 & 0 & K \end{bmatrix} \quad (11)$$

[A] represents the membrane stiffness matrix. In the damaged area, this matrix should be affected by fiber breakages. Generally, these breakages are very localized at the center of the impact, thus the matrix [A] is not modified.

[D] represents the bending stiffness matrix. For thin skins, it is possible to assume the presence of a delamination located at the middle of the thickness and for $R < R_F$. This hypothesis leads to a decrease in bending stiffness. The bending stiffness matrix is divided by four here: [D]/4.

[B] represents the membrane-bending coupling stiffness matrix. When stacking sequences are symmetric with respect to the middle surface, its value is zero. This is not the case for the stacking of the specimen, thus the same hypothesis is used and the coupling stiffness matrix is also diminished: [B]/4.

[K] represents the transverse shear stiffness matrix. It should be affected by matrix cracking but the influence on the residual strength is weak and [K] is not modified.

During the loading, the skin remained linear elastic and no damage growth was modeled. A geometric nonlinear analysis was made using a line-search method. In the next paragraph, the model will be compared with tests performed for which all the data are available in [8]. Typical responses of the first uncrushed springs located on the major axis of the ellipse are given in Fig. 16. Springs representing the undamaged cells reach their peak forces one after another, showing the mechanism of extension of the dent. However, only the load corresponding to the first peak has a physical meaning since it is assumed that there is no damage growth in the skin or appearance of a crack before the dent progression. When the first spring ''crushes'', the computed loading corresponding to the criterion is 291.5 N/mm. The second spring is crushed at 328 N/mm. The experimental failure of this sandwich was at 317.5 N/mm. Thus the criterion under-predicts the failure by about 8%. The out-of plane displacement field for the load criterion can be seen in Fig. 17, showing an extension of the dent in an elliptical shape

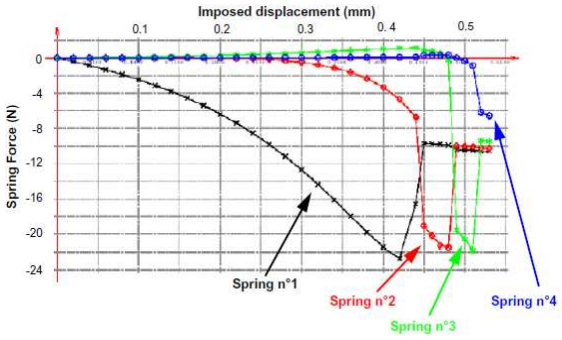

Fig. 16. Typical response given by the model .

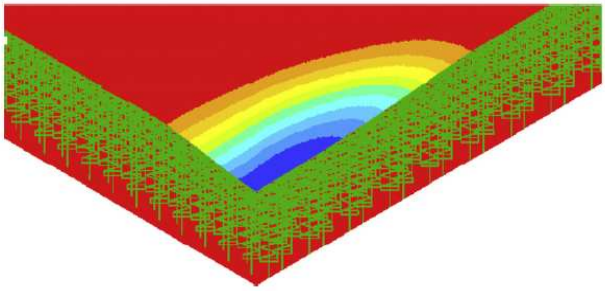

Fig. 17. Shape of the dent at the critical load.

TEST	Impactor Size (mm)	Energy (Joules)	CAI Test (N/mm)	CAI Criterion (N/mm)	Difference
1	25.4	6.7	185.6	162	-12 %
2	76.2	7.2	165.5	150	-9.6 %
3	25.4	6.7	356	413	+ 16 %
4	25.4	20.3	317.5	291.6	-8.15 %
5	76.2	7.2	354.5	265	-25 %
6	76.2	28.2	236.9	196	- 17.3 %
7	25.4	6.7	482.6	600	+ 25 %
8	76.2	11.1	429.6	398	-7.3 %

Table 1: Results given by the core crush criterion

In Table 1, the comparison is given for the 8 cases proposed by Lacy and Hwang [8-9]. Globally, the comparison is good and the residual strength is under-predicted by 8–25%. In two cases (3 and 7), the criterion did not work and over-predicted the experiment by 16

and 25%. The approach seems not to work in the case of low energy impact with small indenters that cause too-small dents. The same behavior was pointed out in the case of metallic skins [4]. Maybe, for small dents, the geometrical imperfections are of the same order of magnitude and should be taken into account. In case n° 5, the residual strength is under-predicted by 25%. The second spring collapses at a load of 315 N/mm (-11%) showing a very progressive extension of the dent. Moreover, for the criterion load, at the apex of the ellipse, the maximum tensile strain is only 8870 µstrains, which suggests that no cracks appear at this load and could explain the value being under-predicted by 25%. In such cases, the analysis should be coupled with modeling of skin damage and failure estimation as proposed in [9] to improve the estimation. However, the present model has the advantage of giving results within 10 min on a personal computer thanks to the use of springs and the linear behavior in the skins. This approach is thus suitable for an industrial context where quick loops are required.

7 Conclusion

An original method for modeling the impact and post-impact behavior of sandwich structures has been proposed and validated. It is based on the demonstration that the Nomex honeycomb behaves in a post-buckling mode very early and that compression forces are taken up by the corners or vertical edges of honeycomb cells in the same way as by the stiffeners in aircraft structures. Thus it is possible to represent the honeycomb discretely by a grid of springs located at the 6 corners of the hexagonal cells. The only experimental characterization for this study is the uniform compression testing on a block of 100 cells to find the law of compression for each corner. This approach represents a third way between very refined models which are able to capture the whole mechanisms of crushing and continuum models which skips a part of the mechanical behaviors.

References

[1] S. Abrate. *Impact on composite structure.* Cambridge University Press, 1998.

[2] Aminanda Y., Castanié B., Barrau J.J., Thevenet P. Experimental analysis and modeling of the crushing of honeycomb cores. *Applied Composite Materials*, vol 12, 3-4, pp 213-227, 2005

[3] Castanié B., Bouvet C., Aminanda Y., Barrau J.J., Thevenet P. Modelling of low energy/low velocity impact on nomex honeycomb sandwich structures with metallic skins. *International Journal of Impact Engineering* Vol 35 pp 620–634, 2008.

[4] Aminanda Y., Castanié B., Barrau J.J., Thevenet P.: Experimental and numerical analysis of the compression-after-impact of metal-skinned sandwich structures. *Composites Science and Technology* Vol 69 pp. 50-59, 2009.

[5] Castanié B., Aminanda Y., Bouvet C., Barrau J.J. Core crush criteria to determine the strength of sandwich composite structures subjected to compression after impact. *Composite Structures* Vol 86, pp 243–250, 2008.

[6] Castanié B, Barrau J.J., Jaouen J.P., Rivallant S. Combined shear/compression structural testing of asymmetric sandwich structures. *Experimental mechanics*, Vol 44, pp 461-472, 2004.

[7] Castanié B., Aminanda Y., Barrau J.J., Thevenet P. Discrete modeling of the crushing of nomex honeycomb core and application to impact and post-impact behavior of sandwich structures, in *Recent Advances in Dynamic Failure of Composite and Sandwich Structures*. S. Abrate, B. Castanié, Y. Rajapakse, Editors, Springer.

[8] Lacy T.E., Hwang Y. Numerical modeling of impact-damaged sandwich composites subjected to compression-after-impact loading. Composite Structures 61 (2003) 115–128.

[9] Lacy T.E., Hwang Y Numerical Estimates of the Compressive Strength of Impact-damaged Sandwich. Journal of Composite Materials 2007; 41; 367.

Copyright Statement